# Soft Matter

Accepted Manuscript






ROYAL SOCIETY OF CHEMISTRY

www.rsc.org/softmatter

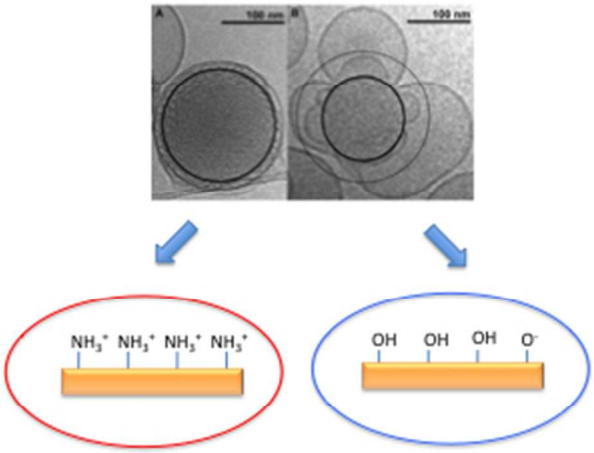


The location of stabilizer (Polysorbate 80) within lipid liquid crystalline nano-particles - neutrons and x-rays reveal internal structure and adsorption.
176x132mm (72 x 72 DPI)

Soft Matter

RSCPublishing

ARTICLE

# Structural effects of the dispersing agent Polysorbate 80 on liquid crystalline nanoparticles of soy phosphatidylcholine and glycerol dioleate

Cite this: DOI: 10.1039/xoxxoooooox

Received ooth January 2012,
Accepted ooth January 2012

DOI: 10.1039/xoxxoooooox

www.rsc.org/

Maria Wadsäter,[a] Justas Barauskas [b,c] Sarah Rogers,[d] Maximilian W. A. Skoda,[d] Robert K. Thomas,[e] Fredrik Tiberg,[a,b] and Tommy Nylander*[a]

Well-defined, stable and highly structured $I_2$ (*Fd3m*) liquid crystalline nanoparticles (LCNP) of 50/50 (wt/wt) soy phosphatidylcholine (SPC)/glycerol dioleate (GDO), can be formed by using a low fraction (5-10 wt%) of the dispersing polymeric surfactant Polyoxyethylene (20) sorbitan monooleate (Polysorbate 80 or P80). In the present study we used small angle neutron scattering (SANS) and deuterated P80 (d-P80) to determine the location and concentration of P80 within the LCNP and small angle x-ray scattering (SAXS) to reveal the internal structure. SANS data suggests that some d-P80 already penetrates the particle core at 5%. However, the content of d-P80 is still low enough not to significantly change the internal *Fd3m* structure of the LCNP. At higher fractions of P80 a phase separation occurs, in which a SPC and P80 rich phase is formed at the particle surface. The surface layer becomes gradually richer in both solvent and d-P80 when the surfactant concentration is increased from 5 to 15 %, while the core of the particle is enriched by GDO, resulting in loss of internal structure and reduced hydration. We have used neutron reflectometry to reveal the location of the stabiliser within the adsorbed layer on an anionic silica and cationic (aminopropyltriethoxysilane (APTES) silanized) surface. d-P80 is enriched closest to the supporting surface and slightly more so for the cationic APTES surface. The results are relevant not only for the capability of LCNPs as drug delivery vehicles but also as means of preparing functional surface coatings.

## 1 Introduction

Reversed lipid liquid crystalline nanoparticles (LCNPs) of the cubic micellar ($I_2$) phase have been demonstrated to have large potential in drug delivery applications due to their good drug loading ability and small size, which allows them to penetrate tissue and reach targeted organs. Recently, the formation of well-defined, stable and highly structured $I_2$ (*Fd3m*) nanoparticles of 50/50 (wt/wt) soy phosphatidylcholine (SPC)/glycerol dioleate (GDO), using a low fraction (5-10 wt%) of the dispersing polymeric surfactant Polyoxyethylene (20) sorbitan monooleate (Polysorbate 80 or P80) was reported.[1] The SPC/GDO system compares with the frequently studied nanoparticles based on monoglycerides, such as glycerol monooleate (GMO), which has negligible hemolytic activity and is non-toxic at relatively high doses.[2, 3] This makes them both suitable also for parenteral administration routes, which has been demonstrated in studies of the *in vivo* parenteral delivery of somatostatin, GLP-1, propofol and docetaxel.[3-6]

The surface-active polymeric surfactant P80 disperses the bulk liquid crystals and stabilises the dispersed LCNPs by reducing the surface free energy. The *Fd3m* structure of the bulk 50/50 SPC/GDO phase was previously shown to be preserved in the LCNPs dispersed with 5-10 % P80, although such P80 concentrations, when mixed into the bulk SPC/GDO phase, cause transformations into an intermediate phase structure or phase mixtures.[1, 7] The polymeric surfactant was therefore proposed to reside mainly at the surface of the particles. However, an increased fraction of P80 did indeed result in a reduced lattice constant in the 5-10 % P80 LCNPs and at 15 % P80 the inner structure was eventually transformed into a disordered micellar phase ($L_2$), as shown by small angle X-ray diffraction (SAXD).[1] In addition to the $L_2$ structure, swollen coronas of disordered multiply connected bilayers were apparent also in cryo-TEM images of SPC/GDO particles containing 15-20 % P80.[3, 9] P80 was thus, at high concentrations, suggested to penetrate partially the particles and solubilize lipids, causing a phase separation, which results in an SPC and P80 rich phase that builds up the water rich corona of interconnected lipid bilayers and a GDO rich, disordered and less hydrated particle core.[1] It is clear that the stabilising shell of the particles is not only important for the structure and

stability of the particles, but also for their function as drug delivery vehicles.

In the first part of this study we have for the first time used small angle neutron scattering (SANS) and deuterated P80 (d-P80), in which the hydrogens in the polyoxyethylene chains of the hydrophilic head were replaced by deuterium, to reveal the structure and location of the P80 in the particle. The deuteration alters the scattering of neutrons, without significantly altering the physicochemical properties of the particle, and by using different ratios of $H_2O$ and $D_2O$ additional different isotopic contrasts can be obtained.[10] In fact, by carefully designing a system using selective deuteration of molecules or parts of molecules or by measuring in different isotopic bulk media ($H_2O$, $D_2O$ and a mixture of the two) specific parts of a sample can be highlighted, providing information on local composition and structure. Here, 50/50 SPC/GDO LCNPs prepared using 5, 10 and 15 % d-P80, relative to the lipid mixture, in different solvent contrasts were studied by SANS and small angle X-ray diffraction (SAXD) to reveal the effect of the polymeric surfactant on the core shell structure and internal liquid crystalline phase of the nanoparticles.

In the second part of this study we have used neutron reflectometry to reveal the location of the stabiliser within the adsorbed layer on an anionic silica and cationic (aminopropyltriethoxysilane (APTES) silanized) surface. The interaction of the LCNPs with various interfaces and the consequences for the particle structure and integrity are relevant not only for their capability as drug delivery vehicles but also as means to prepare functional surface coatings. For instance, for LCNPs serving as drug delivery vehicles, adsorption of material to the storage container, catheters and other delivery devices must be minimized, while systems designed for surface modifying applications would require maximal adsorption. Studies of the interaction of different LCNPs with supported model lipid membranes[4, 7, 9, 11, 12], vesicles[2] and blood[2, 13, 14] have helped to explain the characteristic interactions of the particles with biological interfaces and components. We have previously studied the interaction of both SPC/GDO[7, 9] and GMO[11, 15] based LCNPs with silicon surfaces, either in the natural hydrophilic state or rendered hydrophobic or cationic. The aim has been to understand the nature of the forces that drive the adsorption of LCNPs to various simple model surfaces of different surface energy. We found that the fraction of P80 in the dispersion significantly influenced the adsorption to the hydrophilic silica surface. For instance for 40/40/20 SPC/GDO/P80 a 20-35 nm thick layer, corresponding to multilayer structures or structurally deformed particles, was formed. The thickness of the adsorbed layer from particles with slightly lower P80 fraction (42.5/42.5/15 SPC/GDO/P80) was only a few nanometers (~5 nm).[7] Non-electrostatic interactions between the polyethylene glycol (PEG) units of P80 and the silica were suggested to control the formation of the adsorbed layer. However, the structure and composition of the layer formed close to the surface, in terms the content and location of P80, was not known. Here we use d-P80 to reveal its influence on the structure and composition of the adsorbed layer.

## 2 Results and Discussion

### 2.1 Structure of lipid nanoparticles dispersed by d-P80

#### The stabiliser d-P80 reduces the internal structure of lipid nanoparticles

The internal liquid crystalline (LC) structure of the nanoparticles dispersed by 5, 10 and 15 % d-P80 was determined by SAXD (Figure 1). The nanoparticles containing 5 % d-P80 give rise to 9 distinct Bragg reflections (Figure 1) with relative positions √3: √8: √11: √16: √19: √24: √27: √32: √44, which can be indexed as the reflections from a face-centred cubic micellar phase of the *Fd3m* space group.[16] For an increasing fraction of d-P80 (10 and 15 %), the Bragg reflections of the $I_2$ nanoparticles gradually become less distinct and intense and are almost completely lost at 15 % d-P80, indicating increased structural disorder. The 50/50 SPC/GDO nanoparticles dispersed by d-P80 are thus similar, in terms of LC structure and response to fraction of surfactant, to those previously prepared using a commercial h-P80, which also was found to form an $L_2$ phase at 15 % P80.[1] The lattice constant of the cubic micellar structure decreases with increasing fraction of d-P80 and is 18.0, 17.3 and 16.9 nm for 5, 10 and 15 % d-P80, respectively. This is similar to the lattice constants reported for the corresponding h-P80 nanoparticles.[1] The small differences between h- and d-P80 are probably a consequence of small variations in sample composition of the commercially available h-P80 and the d-P80. It can therefore be concluded that the effect of P80 on the nanoparticle structure is expected to be similar regardless of deuteration.

#### SANS reveals the core-shell structure of the P80 micelles

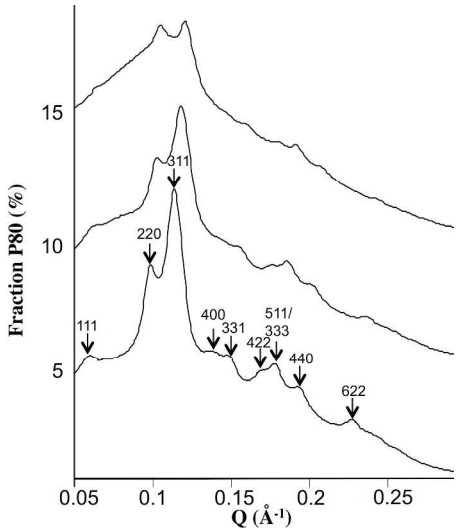


**Fig 1** Small angle X-ray diffractograms of the 50/50 SPC/GDO nanoparticles dispersed by 5, 10 or 15 % d-P80 from bottom to top, respectively, at 25 °C. The indices correspond to the face-centred $I_2$ phase (*Fd3m*).

P80 forms micelles in water and the critical micellar concentration in pure water was previously reported to be 0.014 mM.[17] To extract the degree of deuteration in the head group, d-P80 micelles were studied by SANS in two solvent contrasts, $H_2O$ and 1:1 volume fraction $H_2O$:$D_2O$, (Figure 2). The data were fitted to a core-shell model and the fitting parameters are given in Table 1 for $H_2O$ and 1:1 $H_2O$:$D_2O$ contrasts.. The core is composed of the hydrophobic acyl chains, which is surrounded by a shell of hydrophilic head groups, The volume fraction of solvent in the shell □of the d-P80 head-group were calculated to be around 50% (Table 1). Furthermore, the fitted volume fraction of micelles is consistent with that calculated for a 0.5 % d-P80 micellar solution, verifying the model used for the fitting of the SANS data.. The scattering length density, $\rho$, extracted from the fit for the d-P80 molecule were used in the further analysis of the LCNP dispersions (Table 5). It is noteworthy that value of $\rho$ obtained for the headgroup is between that expected for hydrogenous and completely deuterated polyoxyethylene (20) sorbitan ($1.1 \cdot 10^{-6}$ and $9.5 \cdot 10^{-6}$ Å$^{-2}$)[17], i.e. the average degree of deuteration in the heads was calculated to be 56 ± 5 %.

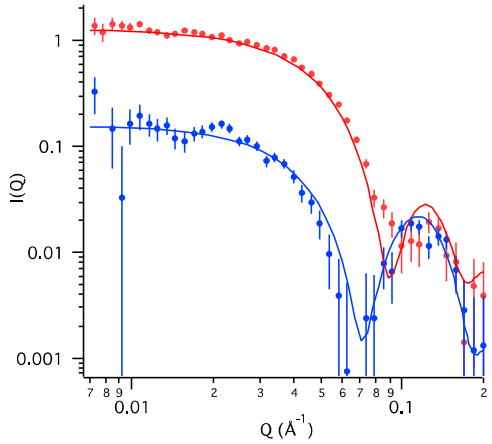


**Fig 2** SANS data of 0.5 % d-P80 micelles in $H_2O$ (red) and 1:1 $H_2O$:$D_2O$ (blue). The fit of the model in Table 1 is shown as solid lines.

**Table 1.** The model fits (in Figure 2) to the SANS of 0.5 % d-P80 micelles in $H_2O$ and 1:1 $H_2O$:$D_2O$.

| | $H_2O$ | 1:1 $H_2O$:$D_2O$ |
|---|---|---|
| Volume fraction of micelles (%) | 3.8 ± 0.4 | 3.8 ± 0.4 |
| Average core diameter (Å) | 42 ± 3 | 42 ± 3 |
| Core polydispersity | 0.05 ± 0.05 | 0.05 ± 0.05 |
| Shell thickness (Å) | 25 ± 3 | 25 ± 3 |
| Volume fraction of solvent in shell (%)[a] | 52 ± 6 | 52 ± 6 |
| Volume fraction of solvent in core (%)[b] | 12±2 | 12±2 |
| $\rho$, core (Å$^{-2}$) x $10^{-6}$ | -0.3± 0.04 | 0.1± 0.03 |
| $\rho$, shell (Å$^{-2}$) x $10^{-6}$ | 2.5± 0.2 | 4.3± 0.2 |
| $\rho$, solvent (Å$^{-2}$) x $10^{-6}$ | -0.56 | 2.90 |
| Background (cm$^{-1}$) | 0.005 | 0.001 |

[a]Based on the $\rho$□of the d-P80 head-group fitted to 5.8± 0.4•$10^{-6}$ Å$^{-2}$, i. e. between what is expected for hydrogenous and completely deuterated polyoxyethylene (20) sorbitan, i.e. 1.1•$10^{-6}$ and 9.5•$10^{-6}$ Å$^{-2}$, assuming a volume of 1085 Å$^3$ for the P80 head group.[17]

[b]Fitting to the two contrast gives an the $\rho$□of the P80 acyl-chain of 2.6±0.2•$10^{-6}$ Å$^{-2}$

## SANS REVEALS A NARROW SIZE DISTRIBUTION AND INTERNAL STRUCTURE OF LIPID NANO-PARTICLES

SANS was used to reveal the effect of P80 on the core-shell structure and composition of the 50/50 SPC/GDO nanoparticles. By using deuterated P80, the scattering length density of the stabiliser surfactant becomes significantly higher than those of the lipids and therefore the presence and location in the particle can be determined.

Figure 3A and B show the scattering profiles from the nanoparticles containing 5, 10 and 15 % d-P80 in 1:4 $H_2O$:$D_2O$ and $H_2O$ together with the fits of the optical model described in Table 2 and 3. All the curves are level off when approaching q ~ 0.001 Å$^{-1}$, showing that the samples contain particles with narrow size distributions and that no or only negligible particle aggregation occurs. At low q (~0.001-0.01 Å$^{-1}$) only small differences in the curves are observed for the nanoparticles with different d-P80 concentrations. At larger q (>0.01 Å$^{-1}$) a fringe appears, whose intensity increases with d-P80 concentration in both the 1:4 $H_2O$:$D_2O$ and $H_2O$ contrast. Finally, Bragg peaks are observed at ~0.11 Å$^{-1}$ and they are particularly intense in the 1:4 $H_2O$:$D_2O$ contrast (Figure 3A). In $H_2O$, the contrast between the lipid and solvent is considerably lower, resulting in weak diffraction peaks. Additionally, the weak peaks are overlapped by a small fringe probably originating from the scattering of P80 micelles (Figure 3D). The Bragg peaks have a similar q-position to that of the most intense 311 Bragg reflection detected by SAXD (Figure 1). Consistent with the 311 Bragg peak, the peak intensity decreases when increasing the d-P80 concentration from 5 to 10 %, while it is almost lost at 15 % d-P80.

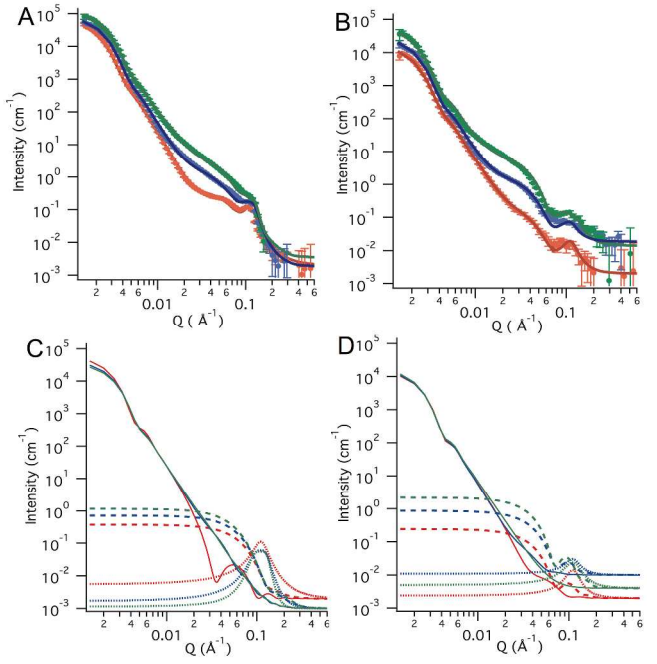


**Fig. 3.** SANS data of 50/50 SPC/GDO nanoparticles dispersed by 5 (red), 10 (blue) and 15% (green) d-P80 in A) 1:4 $H_2O$:$D_2O$ and B) $H_2O$. The fit of the model in Table 2 is shown in A and B (solid lines). The 10 and 15 % d-P80 data sets have been shifted along the y-axis. The components of the model comprise the scattering from NPs (solid lines), micelles (dashed lines) and the diffraction (dotted lines) used in the multi-component model for LCNPs in C) 1:4 $H_2O$:$D_2O$ and D) $H_2O$ are plotted separately.

### Lipid nano-particles have a core shell structure with internal nanostructure consistent with SAXD data

The model fits to the SANS data recorded for the nanoparticles improved considerably when a spherical core-shell model was used instead of simple sphere model, independently of the P80 content. Such a core-shell model is also consistent with cryo-TEM images of the particles. Although, the core-shell model describes the low q data (below ~ 0.01 Å$^{-1}$) very well, the data at larger q (> 0.01 Å$^{-1}$) could only be described by adding the P80 micelle structures to the model (Figure 3C-D). Again, the fits improved when the micelles were modelled as core-shell structures rather than simple spheres.

The inclusion of an empirical broad peak model was required to account for the Bragg peak in the neutron diffraction pattern that the internal *Fd3m* structure gives rise to. The contribution of the broad peak model is also shown in Figure 3C and D. Here it should be noted that a more rigorous modelling of the diffraction pattern is challenging considering that we only observed one Bragg peak within the accessible q-range that was not obscured by the form factor contribution to the scattering pattern.

The total particle diameters (about 1900 Å) obtained from the model fits to the SANS data (Table 2) are similar regardless of d-P80 concentration but are also consistently smaller than those measured by DLS (2202 Å for 5 and 10% and 2750 Å for 15 % d-P80), see Figure ESI:1 in supporting information. The difference in size yielded by the two techniques is not surprising as SANS data gives the radius of gyration while DLS measures the hydrodynamic radius. It is also noteworthy that the polydispersities (0.2-0.3) of the nanoparticle cores obtained from the fits (Table 2) were found to be similar to those obtained from DLS measurements (Figure ESI: 1).

The thickness of the LCNP shell increases with increasing d-P80 concentration in parallel with changes in the $\rho$ of the shell that increases in the 1:4 $H_2O$:$D_2O$ contrast (Table 2). It is however almost constant in the $H_2O$ contrast. Here we note that in 1:4 $H_2O$:$D_2O$ an increased fraction of solvent and d-P80 relative to the lipid content will both increase $\rho$ of the particle shell, since $\rho$ of 1:4 $H_2O$:$D_2O$ and d-P80 is $4.98 \cdot 10^{-6}$ and $3.94 \cdot 10^{-6}$ Å$^{-2}$, respectively. However, in the $H_2O$ contrast, an increased fraction of solvent ($\rho$ of $H_2O$: $-0.56 \cdot 10^{-6}$ Å$^{-2}$) will lower the $\rho$ of the shell and can thus cancel out the effect of an increased fraction of d-P80. Consequently, the fitted $\rho$ of the shell in the two contrasts suggest that it becomes gradually richer in both solvent and d-P80 with increasing d-P80 concentration. In fact this corresponds to the low density shell of lamellar structures, which is particularly apparent in cryo-TEM images for nanoparticles prepared with high fraction of (≥15 %) P80 (see Figure 4).[3, 7-9]

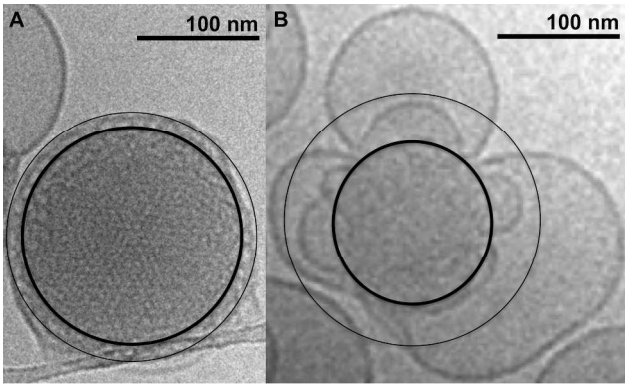


**Figure 4.** Cryo-TEM images of typical 50/50 SPC/GDO nanoparticles dispersed by A) 5 and B) 20 % P80. The fitted model to the SANS data of the nanoparticles comprise a dense core (defined by the thick line in the cryo-TEM images) and a solvent rich shell (defined by the thin line). According to the SANS fit, the core shrinks in diameter and shell increases in thickness with increasing P80 concentration, as is illustrated in the cryo-TEM images.

### Increasing stabiliser P80 concentration increases thickness of shell on the expense of core – core enriched in GDO and shell in P80

We previously suggested that d-P80 induced phase separation, which causes depletion of SPC from the core and the formation of the corona that leaves the core more enriched in GDO.[1, 7] Consistent with the enrichment of GDO in the core and consequently lower degree of hydration, the lattice parameter obtained from SAXD data (Figure 1) and the fitted particle core diameter decrease with increasing d-P80 concentration (Figure 4, Table 2)

.

**Table 2.** The fits of the core-shell models (shown in Figure 3 A and B) to the SANS data from 50/50 SPC/GDO dispersions with 5, 10 and 15 % d-P80 in $H_2O$ and 1:4 $H_2O$:$D_2O$.

| | 5% d-P80 | | 10% d-P80 | | 15% d-P80 | |
|---|---|---|---|---|---|---|
| **LCNPs** | **$H_2O$** | **1:4 $H_2O$:$D_2O$** | **$H_2O$** | **1:4 $H_2O$:$D_2O$** | **$H_2O$** | **1:4 $H_2O$:$D_2O$** |
| Volume fraction of LCNPs (%) | 5.8 ± 0.6 | 1.1 ± 0.14 | 5.5 ± 0.5 | 1.05 ± 0.05 | 5.0 ± 0.5 | 0.95 ± 0.1 |
| Average core diameter (Å) | 1740 ± 100 | 1740 ± 100 | 1560 ± 80 | 1560 ± 80 | 1560 ± 80 | 1560 ± 80 |
| Core polydispersity | 0.22 ± 0.05 | 0.22 ± 0.05 | 0.25 ± 0.03 | 0.25 ± 0.03 | 0.27 ± 0.04 | 0.27 ± 0.04 |
| Shell thickness (Å) | 90 ± 10 | 90 ± 10 | 155 ± 30 | 155 ± 30 | 180 ± 30 | 180 ± 30 |
| Total particle diameter (Å) | 1920 ± 120 | 1920 ± 120 | 1870 ± 140 | 1870 ± 140 | 1920 ± 140 | 1920 ± 140 |
| $\rho$ core (Å$^{-2}$) x $10^{-6}$ | 0.25 ± 0.10 | 0.80 ± 0.15 | 0.30 ± 0.05 | 0.50 ± 0.10 | 0.30 ± 0.05 | 0.40 ± 0.15 |
| $\rho$ shell (Å$^{-2}$) x $10^{-6}$ | 0.05 ± 0.10 | 3.0 ± 0.5 | 0.15 ± 0.08 | 4.6 ± 0.2 | 0.25 ± 0.05 | 5.1 ± 0.3 |
| **Micelles** | | | | | | |
| Volume fraction of micelles (%) | 0.1 ± 0.02 | 0.22 ± 0.03 | 0.3 ± 0.07 | 0.35 ± 0.05 | 0.55 ± 0.07 | 0.4 ± 0.06 |
| Average core diameter (Å) | 60 ± 6 | 60 ± 6 | 64 ± 6 | 64 ± 6 | 76 ± 4 | 76 ± 4 |
| Core polydispersity | 0.2 ± 0.1 | 0.2 ± 0.1 | 0.25 ± 0.04 | 0.25 ± 0.04 | 0.23 ± 0.05 | 0.23 ± 0.05 |
| Shell thickness (Å) | 18 ± 3 | 18 ± 3 | 18 ± 4 | 18 ± 4 | 18 ± 5 | 18 ± 5 |
| $\rho$ core (Å$^{-2}$) x $10^{-6}$ | -0.3 ± 0.04 | 0.1 ± 0.03 | -0.3 ± 0.04 | 0.1 ± 0.03 | -0.3 ± 0.04 | 0.1 ± 0.03 |
| $\rho$ shell (Å$^{-2}$) x $10^{-6}$ | 2.2 ± 0.2 | 4.5 ± 0.2 | 2.4 ± 0.2 | 4.7 ± 0.2 | 2.6 ± 0.2 | 5.4 ± 0.2 |

**Table 3.** The model fits of the broad peak model (shown in Figure 3 A and B) to the SANS data from 50/50 SPC/GDO dispersions with 5, 10 and 15 % d-P80 in $H_2O$ and 1:4 $H_2O$:$D_2O$.

| **Broad peak model** | 5% d-P80 | | 10% d-P80 | | 15% d-P80 | |
|---|---|---|---|---|---|---|
| **LCNPs** | **$H_2O$** | **1:4 $H_2O$:$D_2O$** | **$H_2O$** | **1:4 $H_2O$:$D_2O$** | **$H_2O$** | **1:4 $H_2O$:$D_2O$** |
| $Q_{position}$ | 0.11 | 0.11 | 0.11 | 0.11 | 0.11 | 0.1 |
| Scale | 0.01 | 0.1 | 0.02 | 0.07 | 0.005 | 0.05 |
| n | 2 | 3 | 2 | 4 | 2 | 9 |
| $\xi$ | 30 | 40 | 30 | 35 | 30 | 30 |

The question arises to what extent d-P80 can penetrate into the core of the particle. Here the fitted values of the scattering length density, $\rho$, can give us some important leads. The $\rho$-values of the particle cores were found to increase slightly with d-P80 concentrations in $H_2O$, while they decrease with an increase in the d-P80 concentration in 1:4 $H_2O$:$D_2O$ (Table 2). Here we note that a fully hydrated reverse micellar phase *Fd3m*[19] in 50/50 SPC/GDO is expected to contain about 12% water, which will correspond to a $\rho$ of $0.11 \cdot 10^{-6}$ Å$^{-2}$ and $0.77 \cdot 10^{-6}$ Å$^{-2}$ in $H_2O$ and 1:4 $H_2O$:$D_2O$ respectively. The observed $\rho$-values of the LCNP cores in the $H_2O$ contrast are thus slightly higher than that expected for the *Fd3m* structure of the SPC/GDO phase. The penetration of d-P80 into the core would indeed cause $\rho$ to increase in the $H_2O$ contrast (e.g. from $0.11 \cdot 10^{-6}$ to $0.60 \cdot 10^{-6}$ Å$^{-2}$ when the d-P80 fraction increases from 0 to 15 %). However, a higher d-P80 concentration would also give a corresponding increase in the $\rho$ for the 1:4 $H_2O$:$D_2O$ contrast (from $0.77 \cdot 10^{-6}$ to $1.27 \cdot 10^{-6}$ Å$^{-2}$), whereas a reduction is actually observed. Thus penetration of d-P80 only cannot explain our results.

As previously mentioned, phase separation has been proposed to occur at higher d-P80 concentrations. This is also expected to cause alteration in lipid composition, i.e. depletion in SPC and a relative increase in GDO. Such a phase would be less hydrated, as is obvious from the phase diagram.[1] A reduced fraction of solvent would not only have the opposite effect on $\rho$ in the two contrasts but also a much greater impact in 1:4 $H_2O$:$D_2O$ than in $H_2O$. Indeed if we assume that the fraction of the respective solvent is decreased from 12 to 5 % in a d-P80 free 50/50 SPC/GDO core, the $\rho$ □□ calculated to decrease in 1:4 $H_2O$:$D_2O$ (from $0.77 \cdot 10^{-6}$ to $0.44 \cdot 10^{-6}$ Å$^{-2}$), while in $H_2O$ it would increase (from $0.11 \cdot 10^{-6}$ to $0.16 \cdot 10^{-6}$ Å$^{-2}$). This is due to the greater difference in $\rho$ between the solvent and the lipids in the $D_2O$ rich contrast. The alteration in lipid composition is however, only leads to negligible reductions in $\rho$ in both contrasts, i.e. ~$-0.03 \cdot 10^{-6}$ Å$^{-2}$ when decreasing the fraction of SPC from 50 to 0 %, in a d-P80 free fully hydrated core. An overview of the absolute effects of the d-P80 concentration, fraction of solvent and the SPC/GDO ratio on the $\rho$ values□of the core is given in Table ESI:1.

The fitted $\rho$ for the nanoparticles dispersed by 5 % d-P80 in $H_2O$, suggests that d-P80 is not only present at the particle surface, but to some extent penetrates the core. Indeed, the $\rho$ of a fully hydrated 50/50 SPC/GDO phase containing 5 % d-P80 relative lipid mixture is calculated to be $0.27 \cdot 10^{-6}$ Å$^{-2}$ (Table ESI:1). However, previous bulk phase studies of the SPC/GDO system in excess water showed that the *Fd3m* structure of the 50/50 SPC/GDO phase had already formed an intermediate phase or phase mixtures at 5 % P80.[7] As a distinct inner *Fd3m* structure was observed by SAXD for the 5% d-P80 LCNPs (Figure 1), the fraction of d-P80 is probably less than 5 % in the particle core. Here it should be noted that the resolution of the fit does not allow for a more detailed estimation of the fraction of d-P80 solubilized in the core. However, the P80 concentration used was well above the cmc and the monomer

concentration of P80 is expected to be constant even if the total amount of added P80 increases.[20, 21] In 1:4 $H_2O$:$D_2O$, the fitted $\rho$ of the core shows a decreasing trend with increasing d-P80 fraction (Table 2), which probably reflects a considerable decrease in the fraction of solvent in the core, consistent with the reduced lattice constant obtained by SAXD.

We can now conclude that the SANS data support the previously reported indications that a high fraction of d-P80 induces a phase separation, resulting in a GDO rich and less hydrated core surrounded by a SPC and P80 rich corona. In addition some of the d-P80 is probably entering the core of the LCNP.

### The scattering from free P80-micelles probably adds to the lipid nano-particle scattering

Our SANS data could be described by a core shell particle model together with a broad peak model to account for the Bragg peak. However, it is clear that there is an additional feature at q:s below the single Bragg peak. One possibility was to include the presence of coexisting micellar-like structures in the dispersions, which indeed increase the quality of the model fit to the SANS data (Figure 3 and Table 2). Just as for the pure d-P80 micelles in pure $H_2O$ and 1:1 $H_2O$:$D_2O$ (Figure 2 and Table 1), the micelles present in the nanoparticle solutions ($H_2O$ and 1:4 $H_2O$:$D_2O$) were modelled as core-shell structures. We assume that the scattering length density of the core for the same P80 composition is independent of the presence of SPC/GDO nanoparticles and therefore the values for the pure d-P80 micelles are used.

The fitted $\rho$ of the shell, corresponding to the headgroup region, increases slightly in $H_2O$ and more significantly in 1:4 $H_2O$:$D_2O$ when the d-P80 concentration increases from 5 to 15% (Table 2). The fitted $\rho$ of the shells of the micelles present in LCNP in the 5 and 10 % d-P80 dispersions are slightly lower than for corresponding pure d-P80 micelles in both contrasts. This implies that the micelles are composed of mixtures of d-P80 and non-deuterated lipids. Furthermore, the dimensions of the micelles in the 15 % d-P80 dispersions are not the same as for the pure d-P80 micelles. Solubilized GDO in the micelle cores could be the reason both for their larger core diameter of 67 Å compared to that of the pure d-P80 micelles of 42Å and for the higher polydispersity fitted for the micelles in the dispersions compared to that of the pure d-P80 micelles ($0.05 \pm 0.05$). In addition, the larger shell thickness for the pure micelles of 25 Å than for micelles in the dispersions (18 Å) could also be a consequence of the packing of the lipids and surfactants with differently sized heads and tails in the mixed micelles.

The fitted volume fraction of the micelles in the dispersions increased with d-P80 fraction (Table 2). Indeed, a parallel decrease in volume fraction of LCNPs was indicating a redistribution of the lipid and surfactant material from LCNPs to micelles with increasing d-P80 concentration. The fitted volume fractions of LCNPs are similar to those calculated from the known total composition of the mixture and the assumption of 12 % solvent in the cubic micellar phase of the particles.[19] It should be noted that the fitted concentrations of micelles in the undiluted 5 % and diluted 1% lipid dispersion do not relate to a 1:5 dilution, which suggests that the dilution of the dispersions results in solubilisation of lipids and d-P80 from the nanoparticles and the formation of new micelles. Here we also would like to add that we used a rather primitive model to describe the contribution of the diffraction from the internal structure to the total scattering. In addition, both diffraction from the liquid crystalline phase and scattering from the P80 micelles contribute significantly only to a relatively limited high q part of the total scattering curve. The wider low q part of the scattering curve is dominated by the form factor from the core shell structure of the LCNP. We also cannot rule out that some of the "micellar" entities of "free" P80 micelles at high P80 concentration are in fact attached to the LCNP. Hence the volume fraction of free P80 micelles should not be taken as absolute values, in particular at high P80 concentration.

### 2.2 Adsorption of nanoparticles to hydrophilic and cationic surfaces

Neutron reflectometry (NR) measurements were conducted to reveal the effect of the structure and composition of the layer formed close to the surface, in terms the content and location of P80 in the LCNPs. For this purpose we have made use of deuterated P80, d-P80, in a similar way to that for determining the bulk structure by SANS. The objective with the present study was to estimate whether P80 is enriched in the layer close to the surface and whether there is an effect of surface modification. Two different surfaces were investigated, namely anionic Si/SiO2 and cationic Si/SiO2/APTES substrates. Previous data have shown more extensive adsorption of SPC/GDO/P80 LCNPs on APTES than on silica.[9] Fluorescence microscopy showed that at least some LCNPs do not spread, but remain as intact particles at low density.[7] In a previous study using NR we investigated the adsorption of POPC/GDO/P80 particles on APTES and silica surfaces.[22] There we used high concentrations of P80, namely 15 and 25% of the lipid content. In that case we could not unambiguously determine if there was a particle layer, although we could fit the neutron data to a highly hydrated layer of LCNPs, i.e. 95% solvent. However, a large increase in dissipation in the QCM-D data indeed verified that there were particles on the surface.

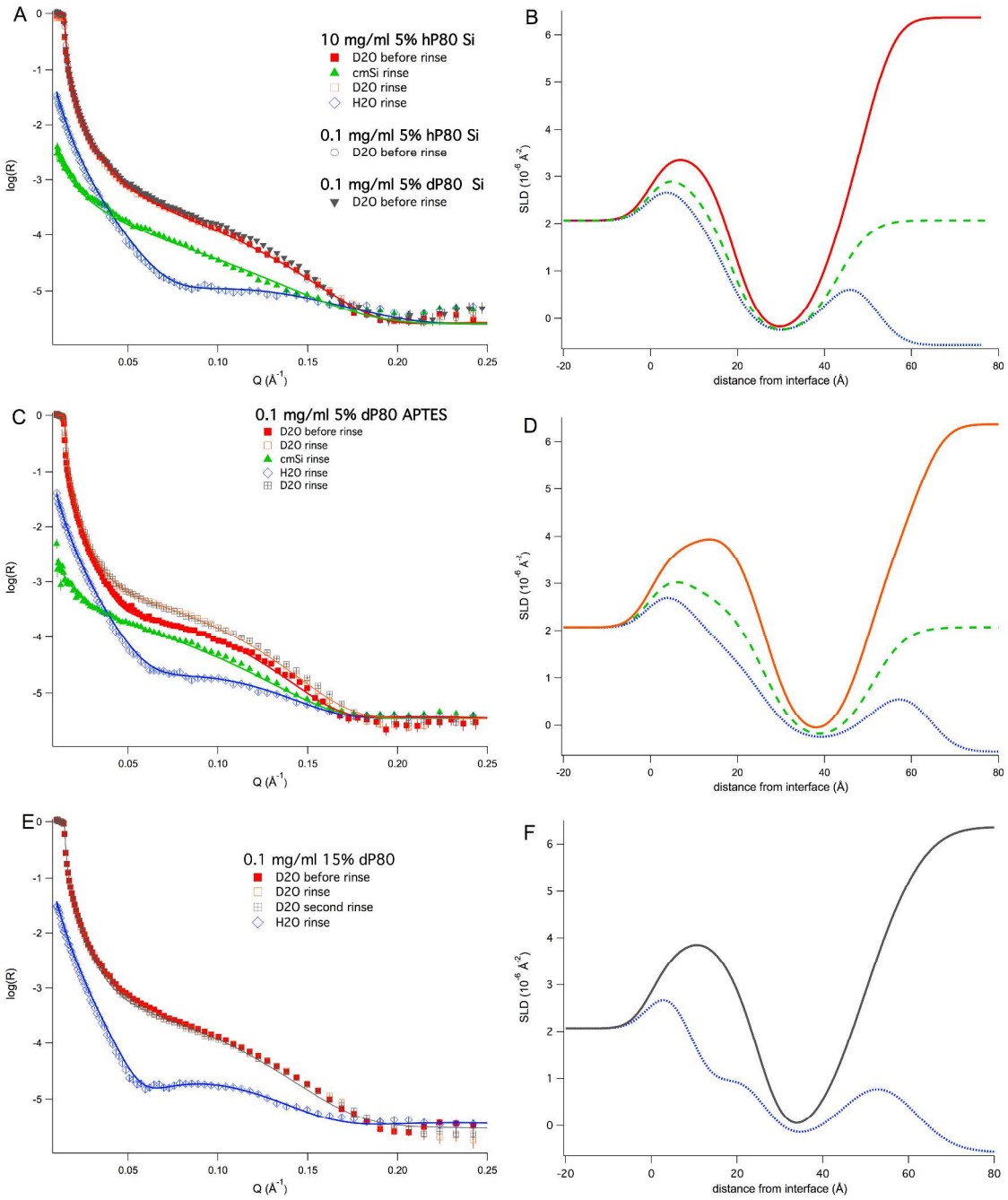


Fig. 5. A) Neutron reflectivity curves from the layer formed upon adsorption of A) 5 % h-P80 or d-P80 50/50 SPC/GDO nanoparticles to a hydrophilic silica surface, C) 5 % d-P80 50/50 SPC/GDO nanoparticles to the cationic APTES surface and E) 15 % d-P80 50/50 SPC/GDO nanoparticles to a hydrophilic silica surface. The corresponding scattering length density (SLD) profiles are given in B, D, and F respectively, where solid line is the profile recorded in $D_2O$, the dashed one cmSi and the dotted line in $H_2O$.

Initial experiments were performed using particles stabilised with 5% h-P80. The reflectivity data recorded in three different solvent contrasts are shown in Figure 5A together with a four layer model ($SiO_2$, lipid head group, acyl chains, head group) fitted to the experimental data and the corresponding scattering length density profile is shown in Figure 5B. The fitting parameters are shown in Table 4. The reflectivity data can also be fitted to a model with an additional thick 100 nm lipid layer with 95% hydration, consistent with our earlier work.[22] However, the improvement of the fit, $\chi^2$, is minute.

When comparing the reflectivity curves in Figure 5A we note that the curve recorded with the LCNPs in the $D_2O$ solution is almost identical to the one recorded after rinsing with $D_2O$

solution. This shows that the layer close to the surface is very stable. We also note that if the surface is exposed to a 100 times larger concentration of LCNPs (10 mg/ml) no difference in reflectivity was observed, which suggests steady state surface coverage is reached already at 0.1 mg/ml. Measurements were also performed using particles prepared with d-P80 were adsorbed from $D_2O$. The fitted values were the same provided we increased the $\rho$ for the lipid head groups in both outer and inner leaflet from 2.0 to 2.9 $\bullet 10^{-6}$ Å$^{-2}$. This increase in $\rho$ indicates that the d-P80 is localised both in the inner and outer leaflet of the lipid bilayer.

The data for the adsorption of LCNPs stabilised by 5% d-P80 on cationic APTES surfaces was also followed by NR and the data were fitted using the same model as for the adsorption on silica surface. Here we note that we cannot distinguish the APTES layer and the $SiO_2$ layer as the APTES layer is expected to be very thin. The recorded data are shown in Figure 5B together with the fits. There are some significant differences compared to the data for silica. First, the layer corresponding to inner leaflet of the bilayer, i.e. the one closest to the surface, is slightly thicker and has a higher $\rho$ than the outer leaflet. This suggests that there is more d-P80 closer to the surface than in the outer leaflet.

Our previous data have shown[7, 9] that we have more intact LCNPs and a large adsorbed amount on the APTES surface. The SANS data discussed above also show that the d-P80 is preferentially localised in the outer shell of the LCNPs. It is then logical to assume that if there is less spreading of material from the particle and/or more intact particles there will be more d-P80 close to the surface. Consequently, we also note that the bilayer is thicker and contains more solvent on the APTES surface than on the silica surface. Furthermore, on the APTES surface we also noticed kinetic effects of the LCNPs adsorption, i.e. the reflectivity curves change with time during the first few hours. Since this was only recorded in one contrast we cannot do any more detailed analyses of changes in layer composition and structure. We observed, however, that the reflectivity curve recorded after 8 h is the same as the one recorded after rinsing with water. This indicates that once steady state is reached the layer seems to be irreversibly bound. We also note that the layer structure was not affected if adsorption took place from $D_2O$ or $H_2O$ solvent.

**Table 4.** Parameters used to fit the model to the NR data reported in Figure 5.

| | Thickness (Å) | $\rho$ ($\bullet 10^{-6}$ Å$^{-2}$) | Solvent (vol %) | Roughness (Å) |
|---|---|---|---|---|
| **5 % h-P80 nanoparticles on hydrophilic $SiO_2$** | | | | |
| SiO2 | 10±1 | 3.4±0.1 | 5.0±0.5 | 7±1 |
| Lipid heads | 9±1 | 2.0±0.1 | 27±1 | 5±1 |
| Lipid tails | 23±1 | -0.30±0.05 | 0±1 | 6±1 |
| Lipid heads | 9±1 | 2.0±0.1 | 27±1 | 5±0.5 |
| **15 % d-P80 nanoparticles on hydrophilic $SiO_2$** | | | | |
| SiO2 | 10±1 | 3.4±0.1 | 5.0±0.5 | 7±1 |
| Layer | 4±1 | 1.0±0.1 | 70±2 | 5±1 |
| Lipid heads | 11±1 | 2.0±0.1 | 30±1 | 5±1 |
| Lipid tails | 22±1 | -0.30±0.05 | 0.0±0.5 | 8±1 |
| Lipid heads | 11±1 | 3.0±0.1 | 30±1 | 8±1 |
| **5 % d-P80 nanoparticles on cationic APTES** | | | | |
| APTES | 10±1 | 3.4±0.1 | 5.0±0.5 | 7±1 |
| Lipid heads | 16±1 | 2.8±0.1 | 40±1 | 6±1 |
| Lipid tails | 25±1 | -0.30±0.05 | 0.0±0.5 | 6±1 |
| Lipid heads | 13±1 | 2.0±0.1 | 45±1 | 5±1 |

In another measurement we studied the adsorption of LCNPs stabilised by a higher content of d-P80, namely 15% d-P80, on silica surfaces (Figure 5E,F). Here we observed some slight changes in layer structure, namely the formation of an inner layer between the supporting surface and the lipid head group of the inner leaflet. The composition of this layer is not clear as it seems to contain something with a rather low $\rho$ value, indicating it is not enriched in d-P80 and it is also hydrated. We noted above when discussing the particle structure that the shell of LCNPs at high d-P80 content not only contained the stabiliser and the solvent, but also contained some lipid material. This probably explains the existence of this extra layer with low $\rho$.

## 3 Experimental

### 3.1 Materials

SPC and GDO were purchased from Lipoid and Danisco, respectively. The purity of the SPC (denoted as SPC S100) was 97.6 % and the hydrocarbon chain composition was 12-17 % palmitic acid, 2-5 % stearic acid 7-12 % oleic acid, 59-70 % linoleic acid and 5-8 % linolenic acid, according to the producer. The GDO (denoted as Rylo DG 20 Pharma) contained minimally 85 % diglycerides and maximally 10 and 5 and 1% mono- and triglycerides and free glycerol, respectively, according to the producer. Furthermore, minimally 89 % of the fatty acids were oleic acid. d-P80 was prepared in Oxford following the procedure described in reference.[23] Ethanol and propylene glycol were purchased from Solveco and Fisher, respectively. Sterile water was obtained from Apoteket (Sweden). Hydrogen peroxide and sulphuric acid for crystal cleaning and APTES, anhydrous toluene and ethanol for surface modification, cleaning and storage were purchased from Sigma Aldrich. All chemicals were used without further purification.

### 3.2 Sample preparation

All sample compositions are given as percentages by weight, unless otherwise stated. SPC and GDO were mixed with ethanol (EtOH) and propylene glycol (PG) (42.5/42.5/10/5 SPC/GDO/EtOH/PG) to reduce the viscosity of the lipid mixture. d-P80 was added to the lipid solution (d-P80/lipid mixture 5/95, 10/90 and 15/90). The lipid solution was then added to sterile water (5/95 (lipid+d-P80)/$H_2O$) followed by

immediate vigorous shaking for 5 days at room temperature. The lipid LC phase samples were thereby coarsely fragmented into homogeneous dispersions, which were further fragmented when passed five times through a Microfluidizer 110S (Microfluidics Corp., Newton, MA) at 5000 PSI. The dispersions were then autoclaved (CertoClav CV-EL, Certoclav Sterilizer GmbH, Traun, Austria) at 125 °C and a pressure of 1.4 bar for approximately 30 minutes and finally filtered using 5 μm Versapor membrane syringe filters (PALL Life Science) to remove any large aggregates, sometimes formed at the aqueous-air interface. The 0.5 % micelle solutions were prepared by solubilizing d-P80 in $H_2O$ and 1:1 $H_2O$:$D_2O$.

### 3.3 Dynamic light scattering

The size distribution of dispersions diluted in $H_2O$ to 0.5 wt% at 25 °C was measured using a DLS (Zetasizer Nano ZS, Malvern Instruments). Autocorrelation functions were analysed using instrument software (Malvern Instruments Ltd.) default General Purpose model and the mean particle size (intensity averaged) and polydispersity was calculated (see supporting information).

### 3.4 Small angle X-ray diffraction (SAXD)

SAXD measurements were performed at beamline I911-4 at MAX-lab, Sweden.[24] Dispersions were injected to capillary cells and bulk LC references loaded to steel sample holders and sealed with kapton windows. The sample was mounted 1952 mm from the 1M PILATUS 2D detector. The x-ray wavelength was 0.91 Å and the size of the beam at the sample was approximately 0.25 x 0.25 mm. Diffractograms of the dispersions were recorded during 3 minutes. The intensities recorded by the 2D detector were integrated using Fit2D provided by A. Hammersley.
(http://www.esrf.eu/computing/scientific/FIT2D/)

### 3.5 Small angle neutron scattering (SANS)

SANS was used to characterize the structure of the 50/50 SPC/GDO nanoparticles and how it is affected by the dispersing agent d-P80. The dispersions of 50/50 SPC/GDO nanoparticles with 5, 10 and 15 % d-P80 were studied in two bulk solvent contrasts, $H_2O$ and 1:4 $H_2O$:$D_2O$. The 5 % micelle solutions were studied in pure $H_2O$ and in 1:1 $H_2O$:$D_2O$. The experiment was conducted at the time-of-flight SANS instrument, SANS2D, at the ISIS pulsed neutron source at the Rutherford Appleton Laboratory in UK. The measurements were made at different two sample-to-detector distances, 4 and 12 m, except for the scattering from neat d-P80 where only 4 meter detector distance was used. SANS2D uses a white neutron beam with wavelengths of 1.75-16.5 Å and 1.75-12.5 Å at respective detector distance, to cover a Q range of ~0.0015-0.6 $Å^{-1}$, where $Q = 4\pi/\lambda \sin(\theta/2)$ and θ is the scattering angle. The bulk solvents were measured using the same setup as for the samples and subtracted from the nanoparticle and micelle sample scattering data. The transmission of the neutron beam was measured on the nanoparticle and micelle samples and bulk solvents, as well as for an empty cell, and the obtained scattering values was used for data reduction. Data were placed on an absolute scale ($cm^{-1}$) using the scattering from a standard sample (a solid blend of hydrogenous and perdeuterated polystyrene) in accordance with established procedures.[25]
The data was analysed using the analysis software SasView.[26] In analysis of SANS data the form factor, P(Q), describes the shape of the particles, while the structure factor, S(Q), describes the inter-particle correlations. However the latter is negligible in dilute samples such as the studied system and was not required to fit the data. The form factor is normalized by the average volume of the particle, V, such that

$$P(Q) = \frac{scale\langle f \cdot f \rangle}{V} + bkg$$

where the scale factor is equal to the volume fraction of the particle and $f$ is the amplitude of the single particle scattering. The scattering intensity is averaged (denoted by < >) over size distribution of the particles, here described by a Gaussian function. The dispersions were analysed with a model where the observed scattering intensities are taken as the sum of the scattering from LCNPs and coexisting micelles. Both the nanoparticles and the micelles were modelled as polydisperse cores with a shell of constant thickness (*CoreShellModel* in the SasView package), for which the form factor is calculated as[27]:

$$P(Q) = \frac{scale}{V_S}\left[3V_c(\rho_c - \rho_s)\frac{[\sin(qr_c) - qr_c\cos(qr_c)]}{(qr_c)^3} + 3V_s(\rho_s - \rho_{solv})\frac{[\sin(qr_s) - qr_s\cos(qr_s)]}{(qr_s)^3}\right] + bkg$$

where $V_s$ and $V_c$ and $r_s$ and $r_c$ are the volumes and radii of the particle and the core, respectively. $\rho_s$, $\rho_c$, and $\rho_{solv}$, are the scattering length densities of the shell, core and solvent, respectively. These can be expressed as

$$\rho = \sum_i \frac{b_i}{V}$$

where $b_i$ is the coherent scattering length of each nuclei $i$ in a given volume, $V$. The $\rho_s$ used in the analysis are listed in Table 5. The core was described by a diameter, $\rho$ and polydispersity. The shell was described only by its thickness and $\rho$ as the fits were found to be insensitive to shell thickness polydispersity, which therefore was excluded from the model. The core diameter, $\rho$ and polydispersity as well as shell thickness and $\rho$ were fitted both for the nanoparticles and the micelles. Furthermore, the core diameter, shell thickness and polydispersity of the nanoparticles and micelles were global parameters and thus the same in the two different contrasts. The volume fraction of both LCNPs and micelles were fitted. Finally, a broad peak model was used to simulate the Bragg diffraction peak. The broad peak was described by the function

$$I(Q) = \frac{scale}{1 + \left(|q - q_{position}|\xi\right)^n}$$

where the scale factor and $q_{position}$ determine the maximum intensity and the position of the peak, while $\xi$ and $n$ gives the shape of the peak.

**Table 5.** The volume and scattering length densities used in the analysis of SANS and neutron reflectivity data.

| Compound | Volume (Å$^3$) | $\rho \cdot 10^{-6}$ (Å$^{-2}$) |
|---|---|---|
| SPC | 1252[18a] | 0.26 |
| GDO | 1104[b] | 0.17 |
| d-P80 | 1577[17] | 3.94 |
| d-P80 head | 1085[c] | 5.82 |
| d-P80 tail | 492[d] | -0.20[e] |
| $H_2O$ | - | -0.56 |
| $D_2O$ | - | 6.36 |
| cmSi | - | 2.07 |
| 1:1 $H_2O$:$D_2O$ | - | 2.90 |
| 1:4 $H_2O$:$D_2O$ | - | 4.98 |

[a]SPC contains a mixture of PC molecules with saturated and unsaturated tails of 16-18 carbons (3.7 % 18:0, 11.4 % 18:1, 63.0 % 18:2, 5.7 % 18:3 and 14.9 % 16:0 PC). This is similar to the egg-PC mixture and the average molecular volume of egg-PC at 20 °C was thus used.

[b]Calculated from the density (0.934 g/cm$^3$) and molecular weight (620.99 g/mol)

[c](Head volume = molecule volume – tail volume)

[d]The volume of the tails in DOPC is 984 Å1 at 30 °C. The volume of the single hydrocarbon tail in P80 is estimated to be the same for the tails in DOPC (984 Å$^3$ at 30 °C[18], 492 Å$^3$/tail).

[e]The value for on DOPC tail[18],

### 3.6 Neutron reflectivity

Neutron reflectometry (NR) was used to study the structure and composition of the layer formed at hydrophilic Si-$SiO_2$ and cationic (silanized) silica upon exposure to the nanoparticle solution. The nanoparticle solutions (0.01 g/ml) were injected into the NR liquid cells and left for at least 10 minutes until steady state adsorption was obtained as verified by constant neutron reflectivity profile. After a steady state was reached, the reflectivity profiles were recorded in three isotopic bulk contrasts: $D_2O$, $H_2O$ and cmSi (contrast matched silicon, 62:38 v/v $H_2O$:$D_2O$), see Table 5. In an NR experiment, the intensity of specular reflected neutrons (R) is measured as a function of the scattering vector (Q) perpendicular to the interface

$$Q = \frac{4\pi}{\lambda} sin\theta$$

where $\theta$ is the angle of incidence and $\lambda$ is the neutron wavelength). The reflected neutron intensity is related to the $\rho$ of the material on the surface via an inverse Fourier transformation.[28] The experiments were performed at the INTER beamline[29] at the ISIS pulsed neutron source at the Rutherford Appleton Laboratory in UK. The measurements were conducted using a white neutron beam (wavelength range 1.5-16 Å) at two fixed incident angles 0.7 and 2.3° to cover a q range from 0.01 to 0.33 Å$^{-1}$. The data were corrected for detector efficiency, transmission, and were then scaled such that total reflectivity ($I = I_{reflected}/I_{incidence}$) obtained at low q in $D_2O$ was equal to 1.

The substrates used throughout this work were polished silicon blocks (15x50x80 mm) purchased from Siltronix (Archamps, France). Before being used, the substrates were cleaned in Piranha solution (3:1 sulfuric acid:hydrogen peroxide) at 80 °C for 10 min. The substrates were then rinsed in MilliQ water and stored in ethanol (>99%) until further use. To investigate the effect of surface charge on adsorption, the silica surfaces were made positively charged by reaction with 3-Aminopropyltriethoxysilane (APTES). The cleaned substrates were dried in an oven to remove any residual water moisture. The substrates were then incubated in anhydrous toluene with 2% 3-aminopropyltriethoxysilane under a nitrogen atmosphere for approximately 2 h. The silanized substrates were then subsequently sonicated in anhydrous toluene and ethanol (3 x 5 min) to remove any unreacted residual materials and finally stored in ethanol until further use.

The analysis of the NR data was conducted using the software Motofit, where the interface is modelled by a stack of thin isotropic layers from which the reflectivity profile is calculated using an Abeles optical matrix method.[30 31] Each layer of the model is described with a layer thickness, $\rho$, interfacial roughness, and solvent fraction. By fitting the simulated reflectivity curve of the layered model structure of the system to the experimental data a $\rho$□profile, and thus the composition, along an axis perpendicular to the interface is obtained. In order to constrain the models, simultaneous fitting of data sets of different isotopic compositions were conducted by using a genetic fitting procedure in Motofit.

The clean Si/$SiO_2$ and Si/$SiO_2$/APTES substrates were pre-characterized by fitting the thickness and roughness of the $SiO_2$ and APTES layer as well as the fraction of solvent in the layers. These parameters were then kept constant in the subsequent fitting process. The LCNPs were found to form lipid/surfactant bilayers at the surfaces. These were modelled as three different layers, the first and third layer representing the lipid heads and the middle layer representing the hydrophobic fatty acid tails, were used to model the lipid bilayer. The thickness, solvent penetration and roughness of each layer were then fitted. In addition a thick extended layer of LCNPs with > 95% solvent could be added to the model.

## Conclusions

For the first time to our knowledge SANS and contrast matching have been used to determine the location of a stabiliser in non-lamellar LCNPs. Here the effect of stabiliser on nanoparticles of 50/50 SPC/GDO was determined using different fractions (5-15 %) of d-P80 and using SANS and SAXD. This study demonstrates that the P80 concentration should be kept as low as possible in order to avoid surfactant-related structurally disordering effects on the particles and minimize the fractions of coexisting mixed surfactant/lipid micelles in the dispersions, while the bulk concentration is high enough to form stable dispersions of the LC phase. A concentration of 5 % P80 was found to be sufficient to disperse the bulk 50/50 SPC/GDO crystal, and SANS data suggests that

some d-P80 penetrates the particle core already for 5% d-P80. However, the fraction of d-P80 solubilized in the interior of the particles is still low enough not to interfere significantly with the internal *Fd3m* structure of the nanoparticles. At higher fractions of P80 a phase separation occurs, in which a SPC and P80 rich phase is formed. This phase relocates at the particle surface and forms a shell of extended, multiply interconnected bilayers, previously depicted by cryo-TEM for SPC/GDO nanoparticles at high fractions of P80. The surface layer becomes gradually richer in both solvent and d-P80 when the surfactant concentration is increased from 5-15 %, while the core of the particle is enriched by GDO, resulting in loss of internal structure and reduced hydration. Besides an inhomogeneous distribution of P80 in the nanoparticles the excess of the surfactant probably exists as P80 micelles, in which also lipids are solubilized.

## Acknowledgements

This work was financed by the Swedish Foundation for Strategic Research (SSF) via framework grant RMA08-0056. We thank the ISIS pulsed neutron source at the Rutherford Appleton Laboratory in UK for allocated beamtime at the Sans2d and INTER beamline. The authors also thank the Swedish synchrotron X-ray facility MAX-lab for allocating beamtime at the I911-4 beamline and Ana Labrador, Sylvio Haas and Tomás Plivelic for technical and scientific support during experiments. We gratefully acknowledge Gunnel Karlsson for her skilled work with the cryo-TEM and Andrew Jackson for valuable discussion on the SANS data evaluation.

## Notes and references

[a] Physical Chemistry, Department of Chemistry, Lund University, P.O. Box 124, SE-22100, Lund, Sweden
[b] Camurus AB, Ideon Science Park, Gamma Building, Sölvegatan 41, SE-22379 Lund, Sweden.
[c] Biomedical Science, Faculty of Health and Society, Malmö University, SE-20506 Malmö, Sweden.
[d] ISIS, Science & Technology Facilities Council, Rutherford Appleton Laboratory, Chilton, Oxon OX11 0QX, United Kingdom.
[e] Physical & Theoretical Chemistry Laboratory, University of Oxford, South Parks Road, Oxford, OX1 3QZ, United Kingdom.

*Corresponding Author Tommy Nylander
E-mail: Tommy.Nylander@fkem1.lu.se

† Electronic Supplementary Information (ESI) available: Figure ESI:1. Size distribution of 50/50 SPC/GDO nanoparticles; Table ESI:1. The theoretical effect of increasing the fraction of d-P80 and solvent in the lipid matrix and the SPC/GDO ratio on the SLD of the nanoparticle core. See DOI: 10.1039/b000000x/

1. M. Wadsäter, J. Barauskas, T. Nylander and F. Tiberg, *ACS Appl. Mater. Interfaces*, 2014, **6**, 7063-7069.
2. J. Barauskas, C. Cervin, M. Jankunec, M. Spandyreva, K. Ribokaite˙, F. Tiberg and M. Johnsson, *Int. J. Pharm.*, 2010, **391**, 284–291.
3. M. Johnsson, J. Barauskas, A. Norlin and F. Tiberg, *J. Nanosci. Nanotechnol.*, 2006, **6**, 3017-3024.
4. C. Cervin, P. Vandoolaeghe, C. Nistor, F. Tiberg and M. Johnsson, *Eur. J. Pharm. Sci.*, 2009, **36**, 377–385.
5. F. Joabsson, M. Johnsson, F. Tiberg and Camurus AB, 2008.
6. C. Cervin, M. Tinzl, M. Johnsson, P.-A. Abrahamsson, F. Tiberg and N. Dizeyi, *Eur. J. Pharm. Sci.*, 2010, **41**, 369–375.
7. D. P. Chang, M. Jankunec, J. Barauskas, F. Tiberg and T. Nylander, *Langmuir*, 2012, **29**, 10688-10696.
8. J. Barauskas, A. Misiunas, T. Gunnarsson, F. Tiberg and M. Johnsson, *Langmuir*, 2006, **22**, 6328-6334.
9. D. P. Chang, M. Jankunec, J. Barauskas, F. Tiberg and T. Nylander, *ACS Appl. Mater. Interfaces*, 2012, **4**, 2643-2651.
10. B. Jacrot, *Rep. Prog. Phys.*, 1976, **39**, 911-953.
11. P. Vandoolaeghe, R. A. Campbell, A. R. Rennie and T. Nylander, *J. Phys. Chem. C*, 2009, **113**, 4483–4494.
12. P. Vandoolaeghe, A. R. Rennie, R. A. Campbell, R. K. Thomas, F. Höök, G. Fragneto, F. Tiberg and T. Nylander, *Soft matter*, 2008, **4**, 2267–2277
13. W. Leesajakul, M. Nakano, A. Taniguchi and T. Handa, *Colloids Surfaces B*, 2004, **34**, 253–258.
14. J. C. Bode, J. Kuntsche, S. S. Funari and H. Bunjes, *Int. J. Pharm.*, 2013, **448**, 87-95.
15. P. Vandoolaeghe, F. Tiberg and T. Nylander, *Langmuir*, 2006, **22**, 9169-9174.
16. J. M. Seddon, *Biochemistry*, 1990, **29**, 7997-8002.
17. M. Ruiz-Peña, R. Oropesa-Nuñez, T. Pons, S. R. W. Louro and A. Pérez-Gramatges, *Colloids Surf., B*, 2010, **75**, 282-289.
18. J. F. Nagle and S. Tristram-Nagle, *Biochim Biophys Acta*, 2000, **10**, 159-195.
19. F. Tiberg, M. Johnsson, J. Jankunec and J. Barauskas, *Chem. Lett.*, 2012, **41**, 1090-1092.
20. R. M. C. Dawson, *Data for Biochemical Research, 3rd ed.*, Oxford University Press New York, 1986.
21. E. L. V. Harris and S. Angal, *Protein Purification Methods: A Practical Approach*, IRL Press at Oxford University Press, New York, NY, 1990.
22. D. P. Chang, A. Dabkowska, M. Wadsäter, R. A. Campbell, J. Barauskas, F. Tiberg and T. Nylander, *Submitted*, 2014.
23. I. M. Tucker, J. T. Petkov, J. Penfold, R. K. Thomas, P. X. Li, C. A. R., N. Hedges and J. R. P. Webster, *J. Phys. Chem. B*, 2014, **118**, 4867-4875.
24. A. Labrador, Y. Cerenius, C. Svensson, K. Theodor and T. Plivelic, *J. Phys. Conf. Ser.*, 2013, **425**.
25. G. D. Wignall and F. S. Bates, *J. Appl. Crystallogr.*, 1987, **20**, 28-40.
26. , SasView, http://www.sasview.org/.
27. A. Guinier and G. Fournet, *Small-Angle Scattering of X-Rays*, John Wiley and Sons, New York, 1955.
28. C. F. Majkrzak, S. K. Satija, N. F. Berk, J. A. Borchers, J. A. Dura, R. Ivkov and K. O'Donovan, *Neutron News* 2001, 25-29.
29. R. A. Campbell, H. P. Wacklin, I. Sutton, R. Cubitt and G. Fragneto, *Eur. Phys. J. Plus*, 2011, **126**.
30. A. Nelson, *J. Appl. Crystallogr.*, 2006, **39**, 273-276.
31. F. Abeles, *Ann. Phys.*, 1948, **3**, 504–520.